Separating Magnetically Labeled and Unlabeled Biological Cells within Microfluidic Channels

Honors Research Thesis

Presented in Partial Fulfillment of the Requirements for Graduation

"with Honors Research Distinction in Physics"

in the Undergraduate Colleges of The Ohio State University

By

Tom Byvank

The Ohio State University

May 2012

Examination Committee:

Project Advisor: Dr. Ratnasingham Sooryakumar, Department of Physics

Dr. Ciriyam Jayaprakash, Department of Physics

Dr. Jeffrey Chalmers, William G. Lowrie Department of Chemical and Biomolecular Engineering

Acknowledgements

Thank you to all the people who have helped me in research and in life.

I especially want to thank Dr. Soory for his mentorship and for giving me the opportunity to conduct this research.

Thanks to all the members of Dr. Soory's group for being great to work with and amazingly helpful, everyone in Dr. Chalmers and Dr. Lee's groups for their collaboration, and the staff of ENSL and Nanotech West for their facilities and training.

Thanks to my family, especially my parents for their encouragement and my existence.

Thanks to my friends, especially Brittany Shrefler, Chris Cannizzaro, Hok Hei Tam and Kevin Rhodus for thought provoking conversations, helping me relax and survive.

Abstract

Within a population, individual biological cells generally have different physical and chemical properties. Research on these differences may affect treatments of diseases and lead to better patient care. We present a technique to separate targeted cells for further analysis. Magnetic micropatterns are used to trap magnetic beads that are specifically attached to targeted cells. The motion of these labeled cells is magnetically controlled within a microfluidic environment, thereby permitting the combination of the cell separation feature with analysis techniques to create an integrated "lab-on-a-chip" device. This miniature unit has the potential for use as a single-cell analysis device or medical diagnostic tool.

The focus of this thesis is the development of a magnetic-trap based mechanism for separating a heterogeneous cell population. Methods for device fabrication and results on optimizing the separation efficiency are presented. Preliminary results of single cell encapsulation, which could be the next step towards realizing the lab-on-a-chip analysis process, are briefly discussed.

Table of Contents

1. Introduction

Analogous to microchips that perform various electronic processes, lab-on-a-chip devices, or micro total analysis systems, are being developed to perform microfluidic functions for engineering and biological applications [1]. These systems allow for efficient and highly controlled analysis of small fluid volumes within low-cost platforms. Integration of reservoirs, pumps and valves permits controlled transportation of the fluid flow within the microchannels (channels having widths on the scale of micrometers, μm). The functionalities of mixing, separation, detection and testing are critical to enable analysis of solutions and their components. Currently, multiple designs of each component of the lab-on-a-chip are being investigated in order to fabricate and develop the most efficient and useful system.

An important feature of microfluidic devices is their ability to manipulate biological material such as cells and viruses within solution. Separation technologies within microfluidic devices are currently being developed because of great interest in the analysis of biological material [2], including rare circulating tumor cells [3]. Integration of any new technologies for biological applications must not damage biological cells while maintaining efficiency. Efficiency in separation technologies can be assessed based on throughput, the rate at which cells flow through the separation area, and purity and recovery rate, reported by the fraction of targeted cells successfully recognized and separated.

Current techniques available for cell sorting include using mechanical, dielectric and magnetic forces. Mechanical systems are, essentially, filters to separate materials based on physical properties such as size [4], and, therefore, have limited applications in

separation of a heterogeneous solution of similarly sized cells. Dielectric mechanisms (dielectrophoresis) are being extensively researched [5], but they present potential problems of intense electric fields damaging biological cells or affecting the cells' molecular properties. Dielectric mechanisms are used within Fluorescent-activating cell sorting (FACS) [6], a macro-scale device used to separate targeted fluorescently labeled cells from unlabeled cells.

Magnetic forces provide a method to sort magnetically labeled and unlabeled cells while using relatively weak fields that will not damage the cells. Current magnetic approaches of separating cells are largely performed with Magnetic-activated cell sorting (MACS) [6], a macro-scale device. These systems efficiently separate cells with high throughput, purity and recovery rate. However, when using the MACS systems, separation is done separately from analysis. Developing magnetic cell separation within microfluidic devices, rather than macro-scale devices, will allow for smaller fluid volumes in low-cost systems and device integration with systems for analysis. Applications for microfluidic magnetic cell sorting devices include single-cell analysis and separation of rare cancer cells from non-cancerous cells for further testing. This analysis is important for studying differences among individual cells within a population.

Enabling the magnetic separation of rare cell populations, Dr. Sooryakumar's research group has developed arrays of structures that can be imprinted with micrometer precision onto a silicon substrate and magnetized [7, 8]. Applying weak tunable external fields to the substrate creates magnetic traps along the arrays. Controlling the external fields permits micrometer precision positioning of the magnetic traps. My project on magnetic cell sorting within microfluidic devices seeks to exploit such external fields and

traps to apply forces on magnetic particles. Cells are sorted using this mechanism by attaching the magnetic particles to targeted cells— thereby "labeling" the cell. Using the magnetic array structures to manipulate the magnetic particles allows for these labeled cells to be separated from unlabeled cells in solution. The unique control provided by the magnetic traps permits simultaneous transport of multiple magnetic structures (i.e. microparticles). The magnetic transport technique allows for remote, programmable and automated cell manipulation. Our system permits control and analysis of targeted biological material to be separated and analyzed within an integrated "lab-on-a-chip" device.

Our research group collaborates with Dr. Jeffrey Chalmer's group in the Ohio State University's Willian G. Lowrie Department of Chemical and Biomolecular Engineering to label magnetic microparticles with specific antigens that permit attachment to the surface of targeted cells [9]. The attached particles and the applied field strengths of less than 150 Gauss do not structurally damage the cells.

Using the most effective parameters for cell separation, the cell sorter will eventually be coupled to a detection platform to be used for cell analysis. The cell sorter will provide the mechanism to obtain the targeted cells to be analyzed. Applications for this lab-on-a-chip microfluidic device would include detection of rare cells with the potential to isolate DNA within the cells that is of value for biological research and medical testing. The device could serve as an inexpensive diagnostic tool, and the low fluid volumes needed for the microfluidic device permit fast processing and analysis of solution.

2. Methods

A. Magnetic Manipulation

The experimental setup is shown in Figure 1. Arrays of magnetic permalloy ($Ni_{0.8}Fe_{0.2}$) disks [5- 10 μm diameter, 40- 80 nm height] are imprinted onto a Si substrate (~2 mm thin ~cm^2 wafer) using electron-beam- or photo- lithography. Four planar electromagnets (Magnetech Corp OP-2025) provide an in-plane magnetic field (H_x and H_y, or $H_{//}$), and a solenoid coil provides a reversible out-of-plane field (H_z) normal to the surface of the Si wafer. The direction and strength of the tunable magnetic fields are remotely controlled utilizing routines programmed in LabView computer software by students in Dr. Soory's group, notably: Tom Henighan, Aaron Chen, Anand Harvind. Magnetic fields up to 150 Oe can be generated using three power supplies (Kepco Bipolar Operational Power Supply/ Amplifier), two for the in-plane fields and one for the out-of-plane field. Experiments are observed through an optical microscope (Leica 10x objective) and are recorded with a high-speed camera (Q Imaging Retiga EXi Fast 1394).

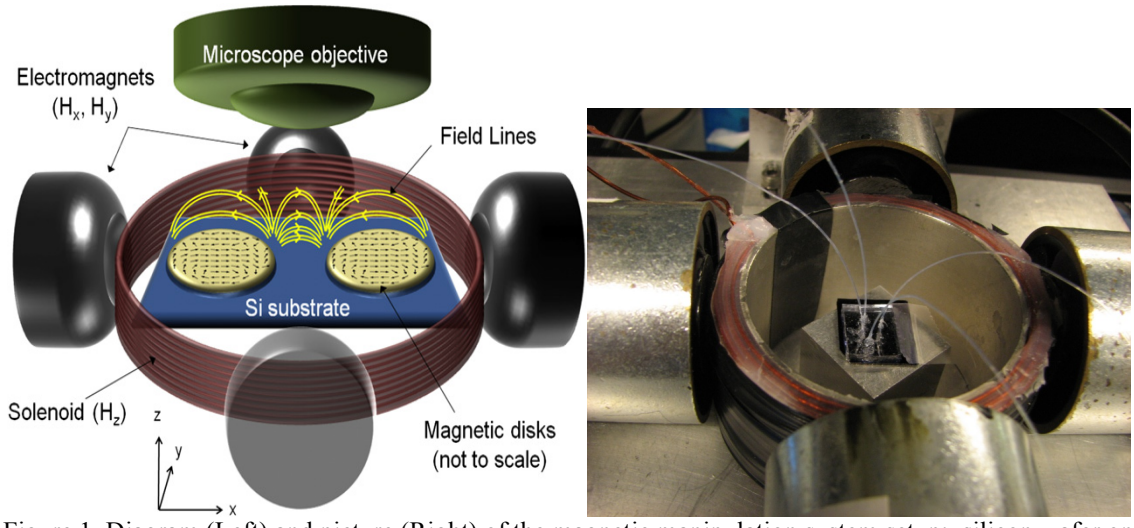

Figure 1. Diagram (Left) and picture (Right) of the magnetic manipulation system setup: silicon wafer on platform surrounded by a solenoid coil, four electromagnets, and below a microscope objective.

The internal magnetic structure of a permalloy disk responding to a 50 Oe in-plane and a 50 Oe out-of-plane magnetic field is plotted in Figure 2. The vector map is calculated with OOMMF simulations. The fields can roughly be compared to a bar magnet parallel with the in-plane external field. The disk's potential energy landscape is also plotted in Figure 2. Magnetic traps form along the circumference of the disk at the location of the potential well.

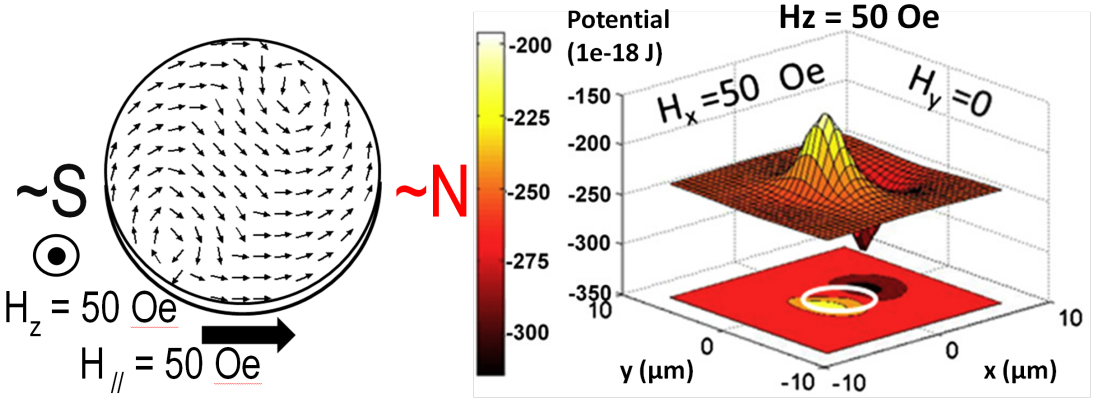

Figure 2. OOMMF simulation of disk's internal magnetic structure (Left). Map of disk's potential energy landscape (Right).

When superparamagnetic beads (polystyrene encapsulated iron-oxide nanoparticles) in solution are introduced into this setup, the external magnetic fields magnetize the particles. The magnetic technique to transport these beads is shown in Figure 3. 1) The beads are held by the disk's magnetic trap. 2-3) Rotating the in-plane external field rotates the position of the disk's magnetic trap, thereby rotating the position of the bead. 4a) Flipping the direction of the out-of-plane external field does not change the magnetic orientation of the disk because it is essentially flat (40- 80 nm). However, this does flip the magnetic orientation of the bead. 4b) The bead will then be repelled (South-South poles) from its current disk and attracted (North-South poles) to a

neighboring disk. The bead does not move back to the opposite side of the original disk due to a potential barrier in the disk's center, as earlier displayed in Figure 2.

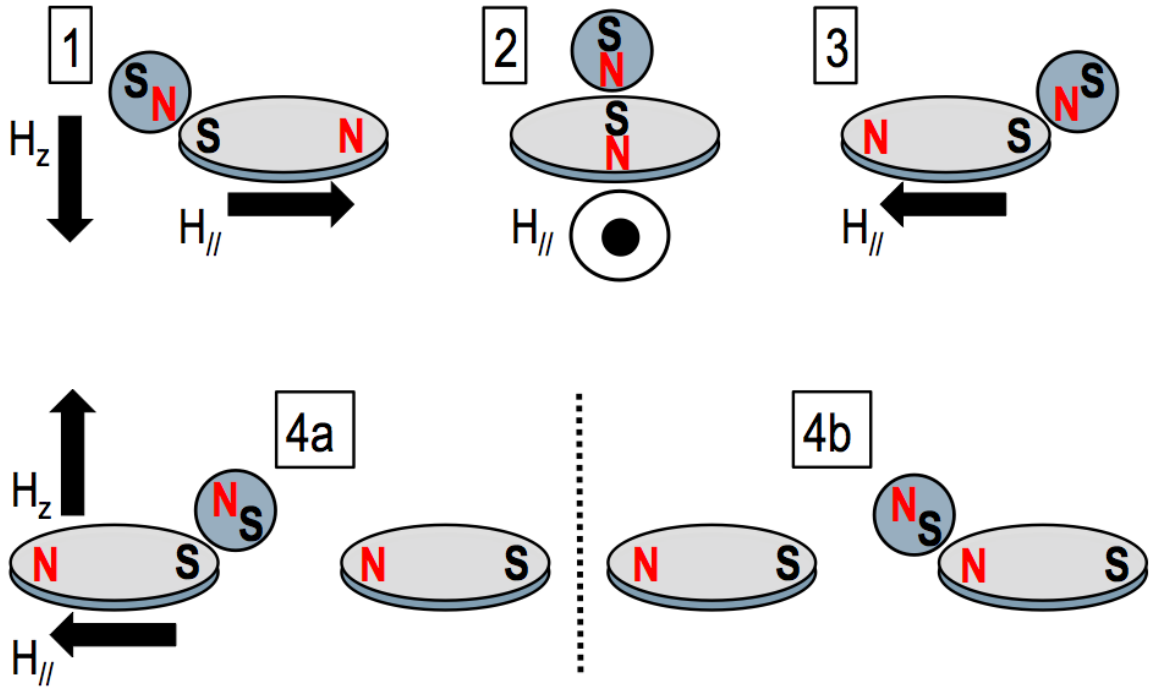

Figure 3. Steps of magnetic bead transportation using external fields and magnetic traps.

B. Cell Labeling

In order to transport them, biological cells are magnetically labeled with superparamagnetic beads as shown in Figure 4. Targeted cells express a specific antigen. For example, some T-lymphocyte white blood cells express the CD3 antigen. Beads are coated with the corresponding antigen to permit attachment to the cell surface. For example, a bead coated with the anti-CD3 antigen may conjugate to the T-cell. The beads act as force transmitting handles for the cell: as the conjugated beads attached to the cell are transported along the disk array, the magnetically labeled cells are also transported. An example of the molecules involved in the labeling process is also shown in Figure 4.

Notably, a polyethylene glycol (PEG) linker (not shown in the diagram) was added within the molecule chain to reduce the tendency for particles (beads) and labeled cells to stick to surfaces within the microfluidic device. We use cells that are typically ~10-15 μm in diameter and labeling beads that are ~2-3 μm in diameter.

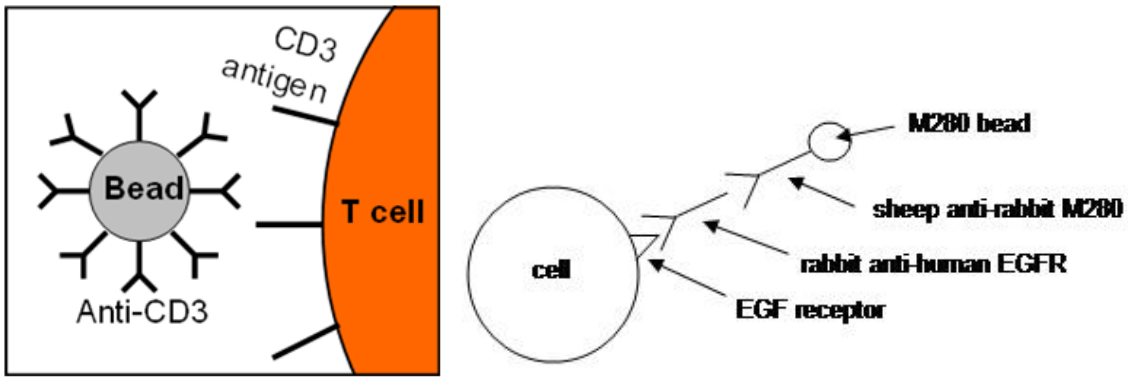

Figure 4. Diagram of antibody- antigen conjugation of bead and cell (Left) and diagram of examples of molecules used for conjugation (Right).

C. Microfluidic Device for Separation and Encapsulation

Fabrication:

See Appendix A for a description of preliminary microfluidic devices used to investigate cell separation. As described below, this device combines the functionalities of separation and encapsulation in droplets within an oil solution for further cell analysis.

To determine optimum design parameters of the microfluidic cell sorter, a photomask (chrome on quartz; Advanced Reproductions) was created with multiple patterns of disk arrays and various microchannel configurations. These parameters are discussed in the results section. The mask was used for photolithography (etching with light) to create disk patterns for sputter deposition and also to produce photoresist microchannel molds. The polymer polydimethylsiloxane (PDMS) was cured over the microchannel molds, forming an impression of a microchannel into the PDMS. To form

the microfluidic device, the PDMS slab was permanently bonded to the Si wafer with the imprinted disk arrays. An overview of the microchannel setup is shown in Figure 5. Aaron Chen and I fabricated this device with Greg Vieira providing help with the sputter deposition. The device was fabricated in the cleanroom at the Ohio State University Nanotech West Lab.

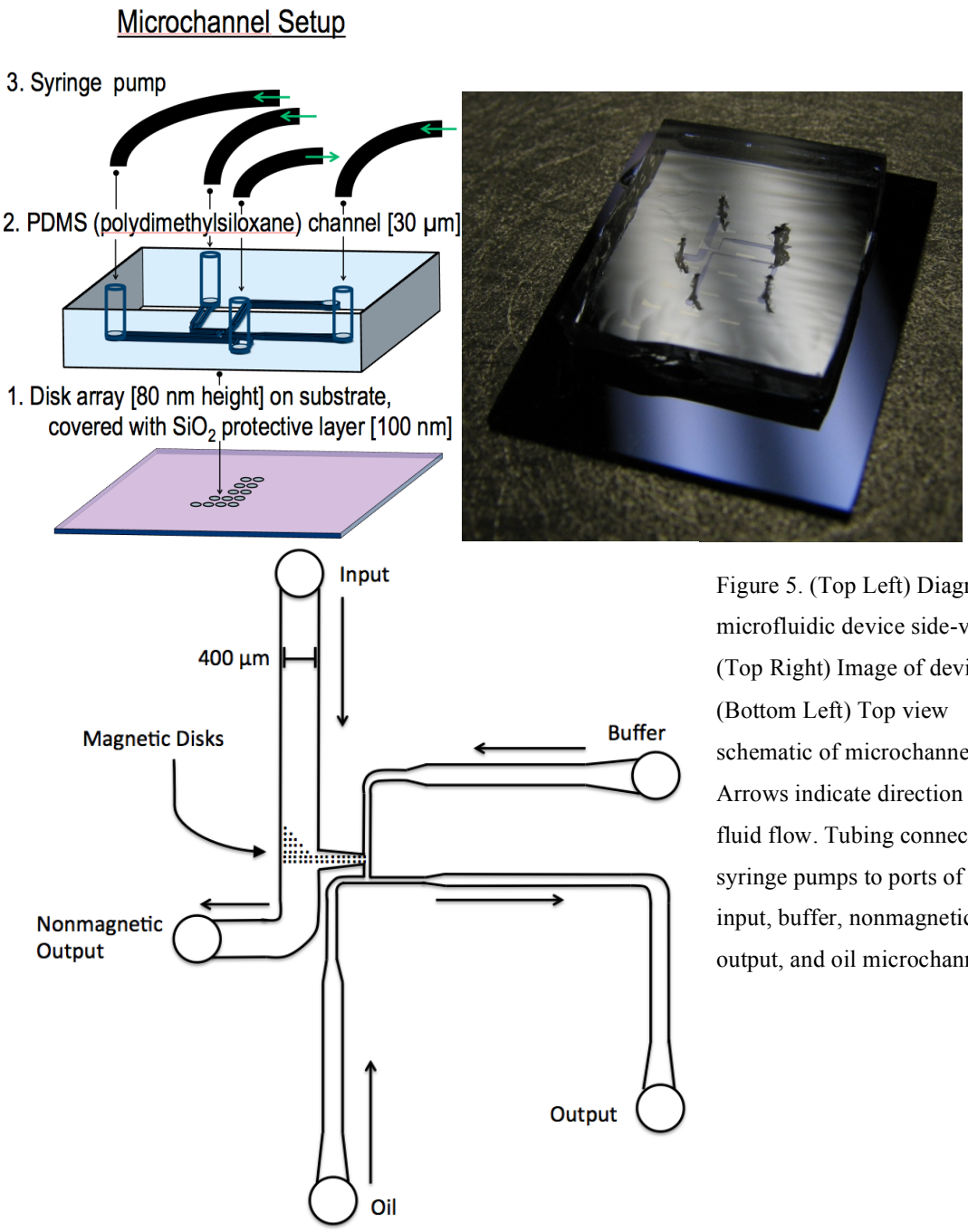

Figure 5. (Top Left) Diagram of microfluidic device side-view. (Top Right) Image of device. (Bottom Left) Top view schematic of microchannel. Arrows indicate direction of fluid flow. Tubing connects syringe pumps to ports of the input, buffer, nonmagnetic output, and oil microchannels.

To produce disk patterns, LOR3B photoresist (MicroChem) was deposited on a Si wafer by spin-coating at 500 rpm for 10 s at an acceleration of 172 rpm/ s, then 2500 rpm for 90 s at 500 rpm/s, and then baked at 180^{o}C for 2 min. Subsequently, S1813 photoresist (MicroChem) was deposited at the same speeds, then baked at 110^{o}C for 90 s. The two layers of photoresist allowed for a more precise and uniform coating during permalloy sputter deposition. The substrate was exposed under UV light for 2.5 s (EV 620 Contact Aligner) and developed with MF-319 for 45 s.

Permalloy was deposited (AJA Sputter Tool) for about 14 min at 1 A/ s, 500 W, 3 mTorr, for a disk thickness of 80 nm. Photoresist and residual permalloy were lifted off with the photoresist remover N-Methyl-2-Pyrrolidone (NMP), leaving only the permalloy disk array. A layer of SiO_2 was then deposited for 21 min at 0.8 A/ s, 500 W, 3 mTorr for a 100 nm protective coating of the disks.

PDMS microchannels were fabricated by curing the material over SU-8 2025 photoresist (MicroChem) molds. SU-8 was spin-coated on Si wafers at 500 rpm for 10 s at 172 rpm/ s and then 3000 rpm for 90 s at 500 rpm/ s. This created a height of 30 μm, allowing for 30 μm-high PDMS microchannels. After waiting a few days for the photoresist to settle, the substrate was soft-baked at 65^{o}C for 3 min and 90^{o}C for 10 min. The photoresist was exposed to UV light for 15 s and then hard-baked under the same procedure as the soft-bake. Subsequently, the substrate was developed in SU-8 developer for 5 min and rinsed with isopropanol (IPA).

PDMS (Slygard 184 Silicone Elastomer Base) was mixed with a curing agent (Slygard 184 Silicone Elastomer Curing Agent) at a 10:1 ratio. Dissolved gasses were removed with a vacuum dessicator. The PDMS was then poured over the SU-8

microchannel molds. After curing for 2 days at room (laboratory) temperature, the PDMS was peeled off. The PDMS microchannel sections were cut into individual pieces and holes were then made to form the ports of the microchannels.

A PDMS microchannel piece was aligned and bonded to the disk array substrate. It was placed bottom side (with the imprinted microchannel) facing up in a Reactive Ion Etcher (Technics Micro-RIE 800) and treated at 40 W, 50 sccm (standard cubic cemtimeters per minute) for 30 s. This process renders the surface hydrophilic by converting a methyl ($-CH_3$) group to a silanol (Si-OH) group; the chemical formula for PDMS is $CH_3[Si(CH_3)_2O]_nSi(CH_3)_3$. Subsequently, within 10 minutes while the surface was still active with the hydrophilic silanol group, the PDMS microchannel was aligned under an optical microscope to overlay correctly with the disk array. The PDMS surface was brought into contact with the Si wafer supporting the disks to form the device, which was then left undisturbed for a few days. The alignment was performed with a device constructed in the lab, allowing for micrometer precision positioning by hand in all directions: vertical up-down, horizontal left-right and front-back, horizontal rotation, tilting left-right and front-back. The PDMS- Si bonding can also be performed by activating the PDMS surface with a 5 min UV Ozone surface treatment, performed in the Photolab at the Ohio State University Center for Electronic & Magnetic Nanoscale Composite Multifunctional Materials (ENCOMM) NanoSystems Laboratory (ENSL). Methanol or ethanol can be used as lubricant for alignment. The device is then baked at 75^oC for 30 min.

Separation and Encapsulation Experiment:

The separation and encapsulation experiment was conducted with biological cells

for proof-of-concept and to allow for further analysis outside of the device. Magnetic and nonmagnetic beads were used for more consistent quantification of device parameters. The experiment was set up with the microfluidic device as in Figure 1 and four syringe pumps (Harvard Apparatus PHD Ultra). To reduce cells or beads sticking to the microchannel bottom, the surface was made hydrophobic with a sigmacote (Sigma-Aldrich SL-2; chlorinated organopolysiloxane in heptane) surface treatment applied for 20 s and subsequently placed on a hotplate at 110^{o}C for 30 min. Another surface treatment option is polyethylene-glycol (PEG) -silane, which is applied for 30 min to 2 hours and then baked for 30 min at 110^{o}C. Tubing (Harvard Apparatus Non-Sterile PolyE Polyethylene) connected four ports of the microfluidic device to the syringes (50 μL Hamilton 1700 Series Gastight) in the syringe pumps. LabView programs controlled the syringe pumps, power supply, magnetic fields and imaging to record the experiments.

Cell solutions contained targeted cells labeled with ~2.8 μm magnetic particles (Invitrogen Dynabeads) and other cells that were magnetically unlabeled. Bead solutions contained 8 μm magnetic particles (Bang Laboratories Compel COOH UMC4N) and 2.3 μm nonmagnetic particles (Spherotech Carboxyl Polystyrene) re-suspended in distilled water (DI) with 0.1% triton (a detergent). For experiments with cells, the buffer solution was phosphate buffered saline (PBS; Mediatech) with 5 g/ L pluronic (a detergent; BASF SE F-68), and oil solution was ionic liquid (Sigma-Aldrich); for experiments with only beads, buffer solution was DI with 0.1% triton, and oil solution was mineral oil (Fisher Scientific 0121-1).

3. Results

A. Experiment

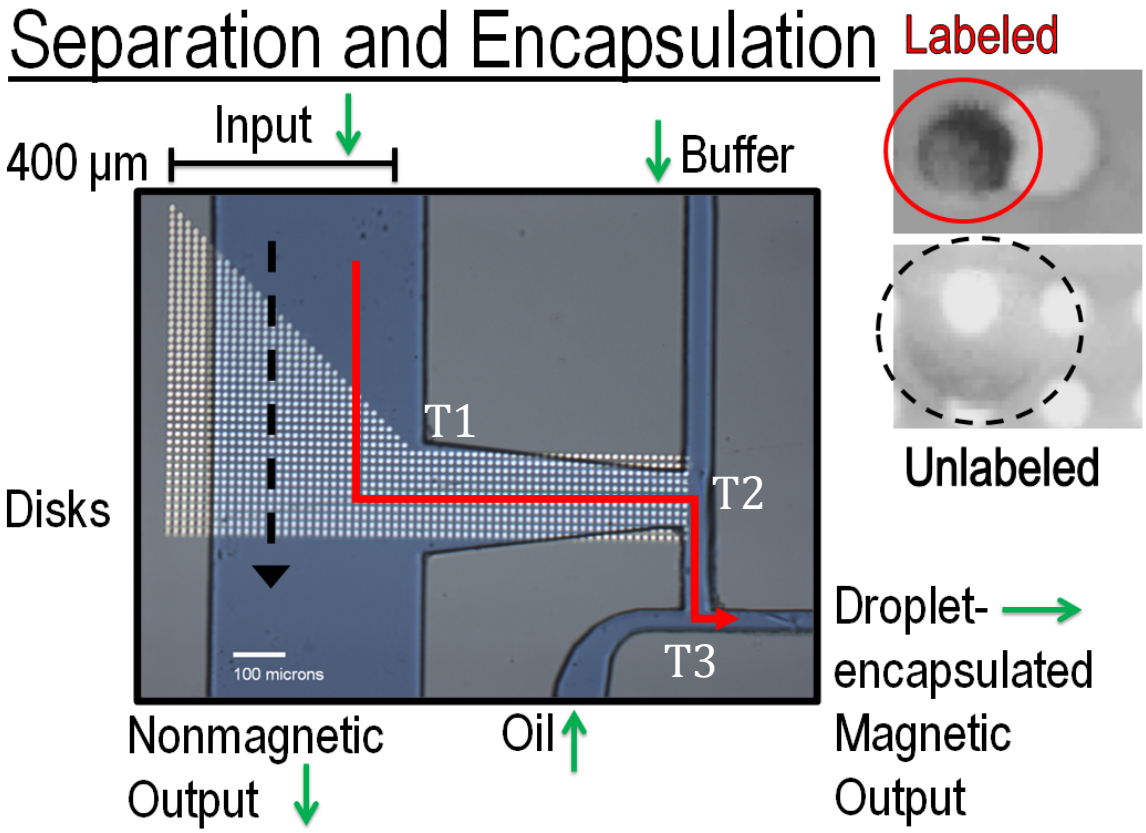

Figure 6. Nonmagnetic material (e.g. unlabeled cells), unaffected by the magnetic disks, follows the dashed black arrow. Magnetic material (e.g. labeled cells), separated from the nonmagnetic material and subsequently encapsulated, follows the solid red arrow.

The solution was introduced into the input port of the device. At a T-shape junction T1 within the device, the solution passed over the disk array. As shown in Figure 6, fluid flow caused nonmagnetic particles/ beads to flow past the disks toward the nonmagnetic output port, and the disk's traps transported magnetic beads into the collection channel (connecting the input/ nonmagnetic output microchannel with the buffer microchannel). At the junction T2 at the end of the collection channel, magnetic beads were pushed by the buffer solution toward another T-junction T3. Here, flow of oil

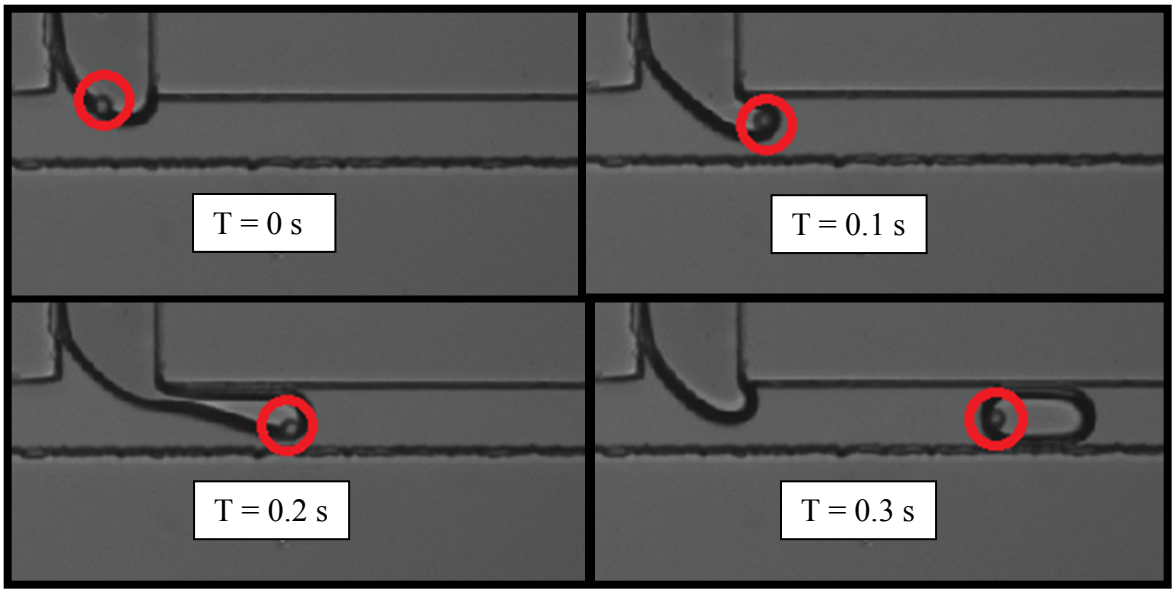

Figure 7. Oil droplet generation and bead (red circle) encapsulation. Oil input flow rate was 50 nL/ min.

(ionic liquid for cells; mineral oil for beads) created droplets of buffer solution and encapsulated beads/ labeled cells within the solution, as shown in Figure 7. The encapsulated magnetic bead is sent to the magnetic output port. Combining the device with on-chip analysis techniques would allow for lab-on-a-chip analysis of targeted material, such as encapsulated single cells. For example, the electrical resistance of oil droplets may be measured to analyze properties of the encapsulated cells. The device has been used to successfully separate labeled and unlabeled Raji cells (leukemia cell line) and BT474 cells (breast cancer cell line). The next step is to work with cancer patient samples to separate the circulating tumor cells.

For proof of concept, cell separation was performed at low flow rates and low rates of transport along the disk array (1 second from one disk to the same location on an adjacent disk). It was found that smaller single cells were more effectively separated than larger cells or clumps of cells. At an input fluid flow rate of 50 nL/ min, 81% of cells with diameters less than or equal to 15 μm were separated, while only 36% of cells with

diameters greater than 15 μm were separated. Factors that contributed to this difference include a higher fluid drag force on the larger cells, which caused them to be knocked off of the magnetic traps. Additionally, larger cells with multiple beads spanned multiple disks and were trapped on different magnetic disks, which reduced the ability for the traps to consistently manipulate the larger cells.

B. Microchannel Architecture

Optimization of the parameters of the microfluidic device will now be discussed. Dimensions of the microchannels affect fluid speed through the channels. The channel height needed to be larger than a few cell diameters (1 cell is ~10-15 μm) to prevent cells or clumps of cells from clogging the microchannel. Too high of a channel would reduce the trapping strength of the magnetic field gradient from the disks, causing them to not trap magnetic beads or labeled cells flowing at the top of the channel. Channel widths must also be larger than a few cell diameters to prevent clogs. Larger widths reduce fluid flow speed (length/ s) for a given fluid flow rate (volume/ s). Lower flow speeds give magnetic disks more time to trap targeted entities, but larger channels require larger disk array sections across the channel width. The larger area means the magnetic objects may have more distance to travel along the disk array. This longer distance and longer travel time means there is a greater probability of viscous drag forces to knock the object off of the traps—especially when "jumping" from trap to trap. Furthermore, a longer distance means greater chance the bead/ cell gets entrapped on the traps, causing further problems within the microchannel like clumps and clogs.

To maximize ability to trap magnetic material while limiting fluid flow into the

collection channel (so nonmagnetic particles are not transported with the magnetic beads), a narrowing collection channel (number 3 in Figure 8) was fabricated. As described in Figure 8, this narrowing allowed more rows of disks to trap magnetic beads than in channels without narrowing, while limiting the amount of fluid that enters into the collection channel. The narrowing channel must be designed so as to avoid clogging if the bead hits an angled channel wall, but rather continue to transport beads for subsequent encapsulation.

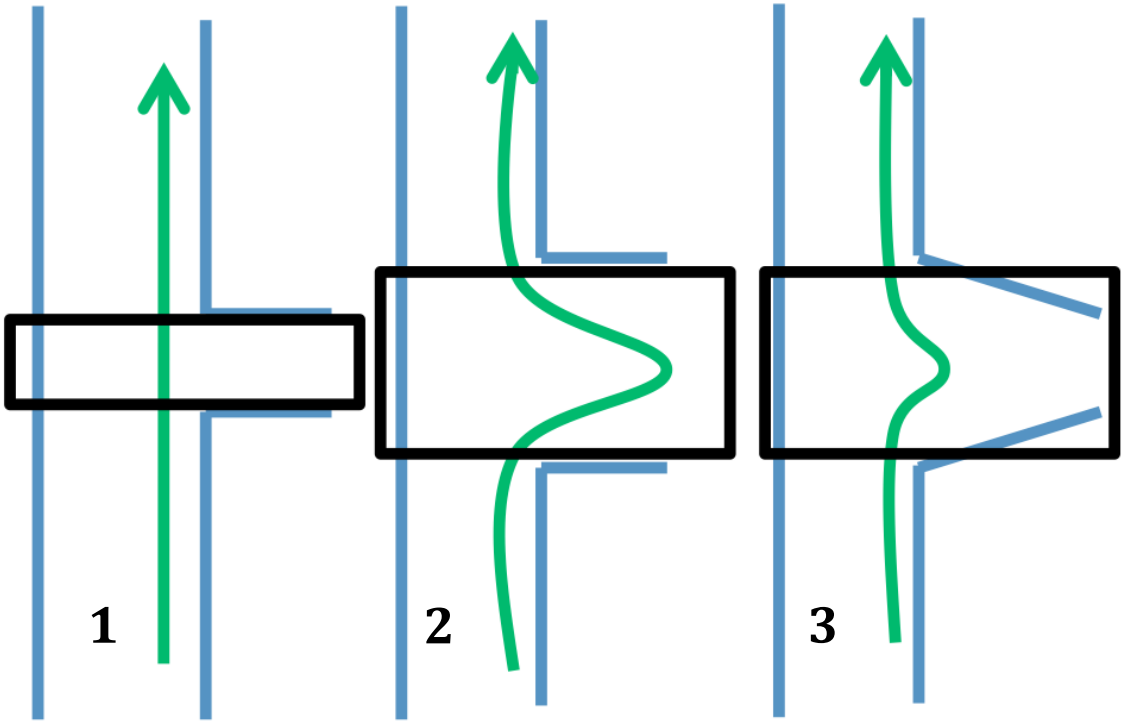

Figure 8. At a microchannel junction (blue), the net fluid flow (green arrow) within the area should be 0. This is essentially due to conservation of mass: the net current (and corresponding volume and mass) going into the junction must equal the net current going out of the junction. In the limiting case (1) with a small branch channel (horizontal blue lines), no flow should enter from the main channel (vertical blue lines). A larger branch channel width (2) allows for the possibility of flow within the branch channel; this has

been observed in the present microfluidic experiments. Fluid flow should deflect less at the narrowing junction (3 vs 2), while still allowing for more disks (within black rectangle) to trap cells (3 vs 1).

C. Magnetic Disk Array Configuration

Multiple rows of disks were constructed to ensure that if fluid flow knocks off particles "mid-jump" while moving from disk-to-disk, there will be additional disks to "re-trap" the particles. Due to their greater magnetic content, 10 μm diameter disks have greater magnetic trap strength compared to that of 5 μm diameter disks. Larger disks require faster movement along the disk circumference for a given field rotation rate, and beads would have a longer distance to travel during the half-rotation between jumps. Shorter spacing between disks allows for quicker "jump" time, so the particles will have less chance to be knocked off by fluid flow. Also, the particles will not "half-jump" as much—not make it all the way to the adjacent disk's trap and return back to the original disk. The exact tendency for this to occur depends on the particle size compared to disk size and spacing.

Two alignments of disks were evaluated: a square lattice array, with disks in-line in a grid of rows and columns; a triangular lattice array, with disks of adjacent rows offset from one another by one disk diameter. Furthermore, a triangle protrusion was added before the T-junction to investigate if it would help give magnetic beads farther away from the collection channel a "head start" to be separated. Differences between microchannel and disk array geometries are shown in Figure 9.

Figure 9. (Top) Picture of straight collection channel with a square lattice array, no triangular protrusion, of 5 μm diameter disks with 5 μm in-between spacing. (Bottom) Picture of narrowing collection channel with a triangular lattice array, triangular protrusion, of 10 μm diameter disks with 10 μm in-between spacing.

D. Separation Efficiency

Specifications for the optimum microchannel for separation of 8 μm magnetic beads were determined to be: 30 μm height, 400 μm main input channel width, 10 μm diameter disks, 5 μm spacing in between disks, square lattice disk array with a triangular protrusion toward the input channel, with a narrowing collection channel. Using microchannels with these specifications, parameters affecting the separation and encapsulation were investigated. As shown in Figures 10, 11 and 12, the "separation efficiency"(fraction of magnetic beads separated into the collection microchannel to total number of input magnetic beads) was affected by parameters including fluid flow rate,

magnetic field strength and rate of transport along the disk array. For these experiments, the solution's concentration of magnetic beads was 1.8 *10^6 beads/ mL.

Error bars for the data in Figures 10, 11 and 12 were determined based on the number of beads knocked off the disk array and the number pushed into the separated buffer channel. The upper bound was calculated as the ((total number of separated magnetic beads)+(beads knocked off))/ (total number of magnetic beads that passed over the disk array). The lower bound was calculated as the ((total number of separated beads)-(beads pushed into separated buffer channel))/ (total number of magnetic beads that passed over the disk array).

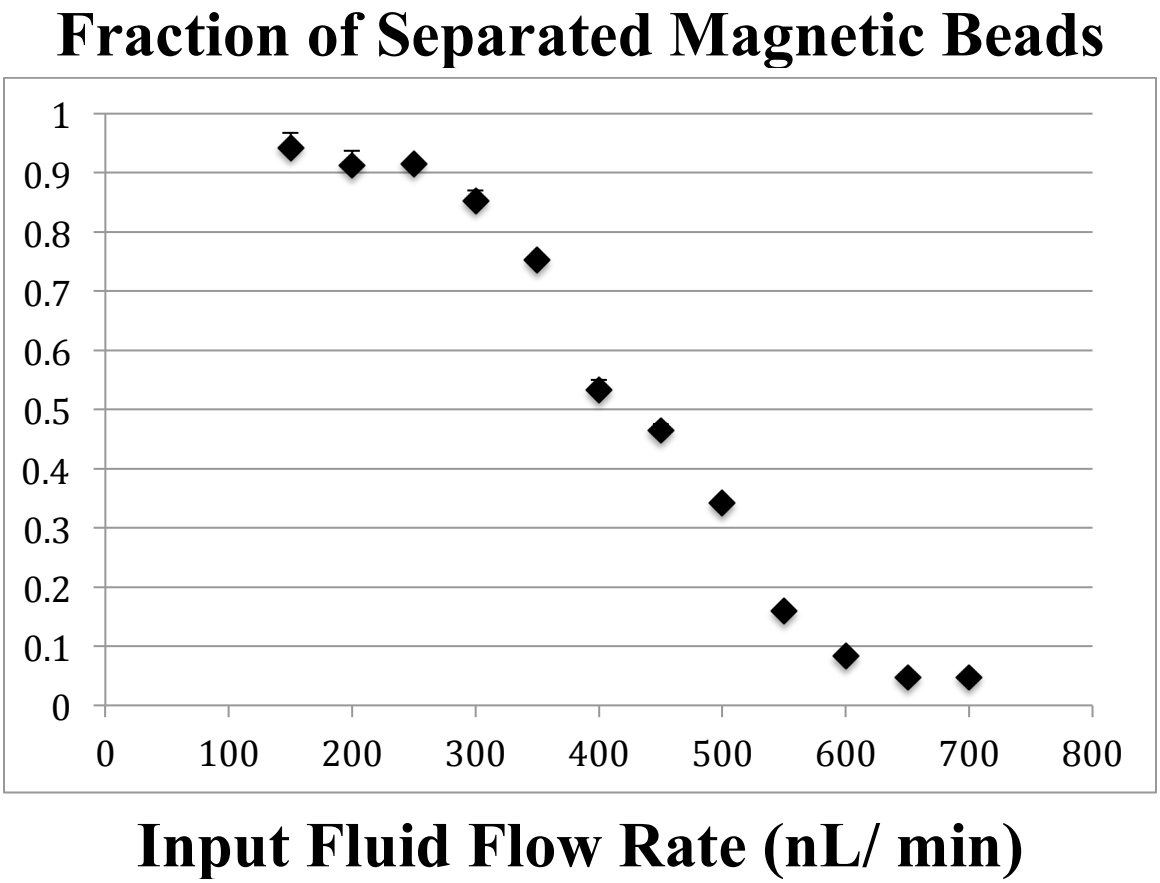

Figure 10. Separation efficiency of varying input flow rates at a 100 Oe in-plane field, a 150 Oe out-of-plane field, and a 5 Hz rate of transport.

A high separation efficiency (>90%) was maintained until an input flow rate of ~300 nL/ min, after which a decrease is separation efficiency is observed. Higher flow rates caused less effective separation due to knocking beads off of the disk array, likely when the beads were in "mid-jump" between two magnetic traps. For this data set, 100 Oe in-plane and 150 Oe out-of-plane magnetic fields were used along with a 5 Hz rate of transport.

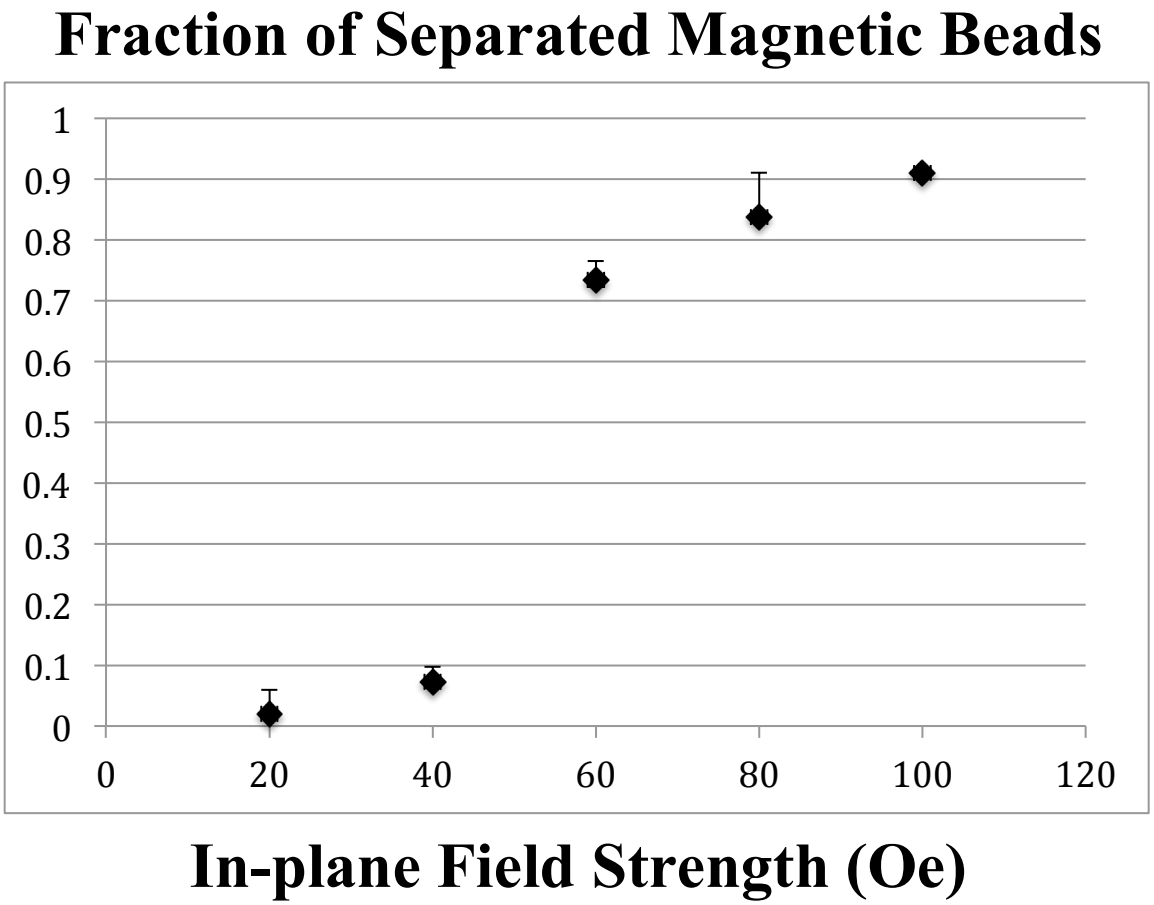

Figure 11. Separation efficiency of varying magnetic field strengths at a 250 nL/ min input flow rate and a 2 Hz rate of transport.

Greater magnetic field strengths were more effective at magnetically separating beads. The in-plane (XY) to out-of plane (Z) field strengths were set at a 2:3 ratio. For example,

the top right point corresponds to 100 Oe in-plane: 150 Oe out-of-plane. For this data set, an input flow rate of 250 nL/ min was used along with a 2 Hz rate of transport.

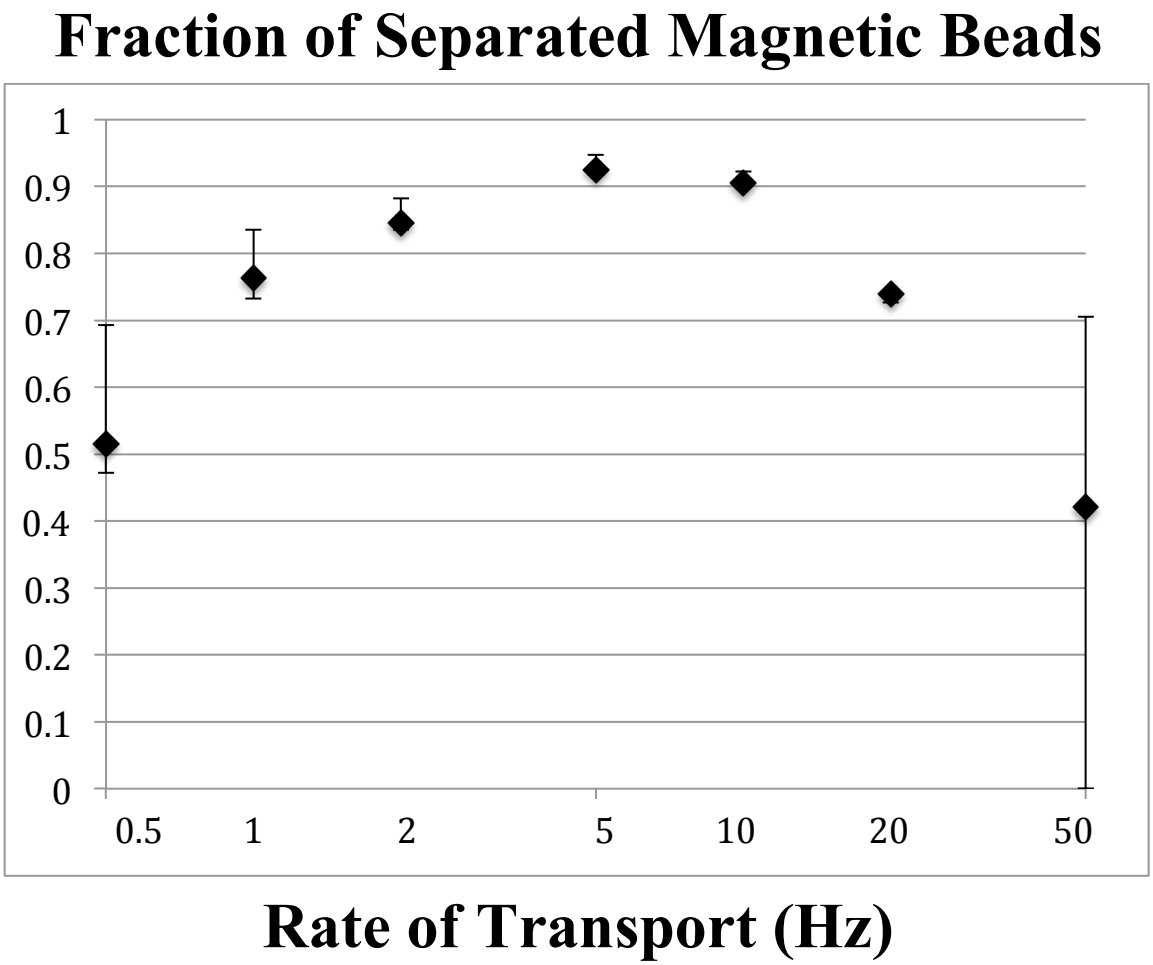

Figure 12. Separation efficiency of varying rates of transport along the disk array at a 250 nL/ min input flow rate, a 100 Oe in-plane field, and a 150 Oe out-of-plane field. Note: The x-axis is plotted on a log scale.

The rate of transport corresponds to time for a trapped bead to travel along a disk's circumference to the opposite end of the disk and then jump to the adjacent disk. A rate of transport of 1 Hz would mean a bead would travel half a rotation around the disk in 0.5 s and then take 0.5 s to jump from the magnetic trap on one disk to the trap on the

adjacent disk, due to the reversing the direction of the out-of-plane field as described by Figure 3.

Faster rates were more effective at separation by more quickly transporting the beads into the collection channel, permitting less time for the fluid flow to potentially knock the beads off of the disk array.

The larger errors at low transport rates are due to beads being knocked off of disks because the disks were saturated with beads.

At too high frequencies, the transport would often "stall", meaning by the time the trap direction was switched by the out-of-plane field, the bead would almost jump to the trap on the adjacent disk, the trap direction would switch again, thereby stalling the bead's motion.

At 2 Hz and 10 Hz, beads were transported at ~30 μm/ s and ~152 μm/ s, respectively. At 20 Hz, when the beads did not stall during their movement, beads were transported at speeds as high as ~285 μm/ s.

E. Magnetic and Fluid Flow Force Comparison

Thanks to Aaron Chen for valuable discussion in regard to the force comparison.

The interplay of fluid viscous drag with magnetic trapping force is important for separation of magnetic beads. Within microfluidic channels, there is laminar flow, and an estimate on the hydrodynamic drag force on a bead, ignoring near-wall effect, is given by Stoke's law:

$$F_d = 6\pi\eta R v$$

where η is the fluid's dynamic viscosity, R is the bead's radius, and v is the bead's speed.

The force on the magnetic dipole of the superparamagnetic bead [8, 10] is due to the gradient in the net magnetic flux B. It is given by:

$$F_m = (1/2)\ \nabla(m \cdot B)$$

where $m = \chi VB/\mu o$ is the bead's induced magnetic moment (assumed linear in B when far below saturation), χ is the bead's magnetic susceptibility, V is the bead's volume, and μo is the free space permeability.

To magnetically trap a bead, the magnetic force must be greater than the hydrodynamic drag force. As a qualitative comparison between these two forces, take an 8 μm diameter magnetic particle (with typical susceptibility $\chi = 0.1$) trapped on the edge of a uniformly magnetized disk (under an external field of 100 Oe in-plane and 150 Oe out-of-plane) as example: the easiest way to free the particle from the asymmetric trap is to pull it along the direction tangential to the disk edge, which requires a force of 120 pN (pulling it along other directions would require 250 ~ 350 pN force). Therefore, a fluid drag force greater than 120 pN is required to knock the particle off the trap under a flow perpendicular to the direction of manipulation, which implies, from Stoke's formula, a critical flow speed of 1600 μm/ s or an equivalent flow rate of 1100 nL/ min in the input channel. Further investigation shows that a drag force of 105 pN (flow of 1400 μm/ s or 1000 nL/ min) is enough to divert the path of the particle during the hopping phase of the manipulation scheme such that the particle is caught by a subsequent disk down the stream, instead.

However, the observed flow rate at which the separation fraction starts dropping is around 300 nL/ min (Figure 10), far below the estimated critical flow rate. This can be attributed to several factors: (a) particles floating above the surface have less time to drop

onto the trapping array under higher flow rate (drop speed is ~3μm/s due to gravity); (b) the amount of trapped particles is limited by the occupancy of the array, which causes loss of particles especially under high flow rate or low manipulation/ transport speed; (c) at high manipulation speed, particles have more chance of not catching up with the moving trap during the hopping phase. Hence, an optimal manipulation speed depends on parameters such as the flow rate, concentration and magnetic moment of the particles.

4. Challenges, Next Steps and Discussion

During cell and bead separation experiments, beads may collect along the microchannel walls. As beads clump, it may clog the microchannel. Cleaning the microchannel at a high flow rate may flush out the clog, but sometimes the channel will remain permanently clogged, requiring new devices. Improving the device durability may allow the microchannel to consistently be reused for experiments. However, devices can be inexpensively mass-produced, which holds promise for future use as medical diagnostic tools.

The microfluidic device only requires small fluid volumes (~microliters) to operate. This is beneficial if the solution volume is limited, but larger fluid volumes will take a longer time to process. In order for large quantities (~milliliters) of fluid to be analyzed, multiple devices may be run in parallel or multiple separation junctions may be run in series for fast and efficient processing of solution.

To increase throughput of cells that travel through the microchannel, a higher fluid flow rate is required. Nonetheless, the fluid flow must not overwhelm the magnetic trapping force from the disks. Although the balance of forces may limit the throughput,

the precise control over the manipulation allows for high (~100%) purity rate: only magnetic beads/ labeled cells will be separated, while all nonmagnetic particles/ unlabeled cells will follow the fluid flow.

Biologically, different cell types have different physical and chemical properties. Therefore, some cells adhere more than others and have different labeling efficiencies because of the number and type of receptors on the cell surface. There are even differences among individual cells of the same type. The cell separation device may permit analysis of these differences, but some cells are easier to separate than others.

The cell separation device may be combined with other functionalities for "lab-on-a-chip" analysis. One limitation of the current cell separation device is that it requires cells to be pre-labeled before the solution is introduced. "On-chip" labeling would allow mixing of cell and bead solutions within a microfluidic device, facilitating attachment of magnetic beads to targeted cells. After cell separation, potential "on-chip" analysis techniques include electroporation, examining the nucleic acid within the targeted cells and injecting chemicals such as biomarkers into the cell membrane. Ultimately, the "lab-on-a-chip" microfluidic device may allow for advances in medical diagnostics, including cancer treatment, for example.

5. Conclusion

Targeted separation of rare cells is important for biological research. When integrated within microfluidic devices, such cell separation has the potential for "lab-on-a-chip" applications. Incorporating microfluidic functions allows for efficient and highly controlled analysis of biological entities, such as cells, within small fluid

volumes. In current techniques based on magnetic cell sorting, improvement is needed in the combination of throughput, purity, recovery rate and the minimum necessary volume of cells in solution. For the purpose of separating different types of cells, in the present research project, targeted cells were labeled by microscopic magnetic particles coated with specific antibodies that permit attachment to the cell surface. The separation was based on remotely manipulating magnetically labeled cells using arrays of magnetic disks imprinted on the surface of a microchannel structure. Utilizing the traps, cells were separated into different channels based on their labeling. Cells were then encapsulated in oil droplets to permit further analysis. The present research has demonstrated that cell populations can be sorted, and further experimentation would lead to such separation on low-cost microscopic portable platforms to be used for cell analysis.

6. References Cited

[1] D. Figeys and D. Pinto, Lab-on-a-Chip: A Revolution in Biological and Medical Sciences, *Anal. Chem*, 72, 9: 330A- 335A (2000).

[2] P. Chen, X. Feng, W. Du and B. Liu, Microfluidic chips for cell sorting, *Front. Biosci*, 13: 2464- 83, 2859 (2008).

[3] M. Zborowski and J. J. Chalmers, Rare Cell Separation and Analysis by Magnetic Sorting, *Anal. Chem*, 83 (21), 8050–8056 (2011).

[3] M. Toner and D. Irimia, Blood-on-a-Chip. *Annu Rev Biomed Eng*, 7, 77-103 (2005).

[4] K. Takahashi, A. Hattori, I. Suzuki, T. Ichiki and K. Yasuda, Non-destructive on-chip cell sorting system with real-time microscopic image processing, *J Nanobiotechnol*, 2: 5,

14773155 (2004).

[5] M. J. Fulwyer, Electronic Separation of Biological Cells by Volume, *Science*, 150: 910–911 (1965).

[6] S. Miltenyi, W. Müller, W. Weichel and A. Radburch, High Gradient Magnetic Cell Separation With MACS, *Cyto*, 11, 2: 231- 238, 990110203 (1990).

[7] G. Vieira, T. Henighan, A. Chen, A. J. Hauser, F. Y. Yang, J. J. Chalmers and R. Sooryakumar, Magnetic wire traps and programmable manipulation of biological cells, *Phys. Rev. Lett.*, 103:128101–128104 (2009).

[8] T. Henighan, A. Chen, G. Vieira, A. J. Hauser, F. Y. Yang, J. J. Chalmers and R. Sooryakumar, Manipulation of Magnetically Labeled and Unlabeled Cells with Mobile Magnetic Traps, *Biophys J*, 98 (3), 412- 417 (2010).

[9] K. E. McCloskey, J. J. Chalmers and M. Zborowski, Magnetic Cell Separation: Characterization of Magnetophoretic Mobility, *Anal. Chem*, 75 (24), 6868- 6874 (2003).

[10] S. S. Shevkoplyas, A. C. Siegel, R. M. Westervelt, M. G. Prentiss and G. M. Whitesides, The force acting on a superparamagnetic bead due to an applied magnetic field, Lab Chip, 7, 1294-1302 (2007).

---

7. Appendix

A. Prototype Photoresist Device

To test the concept of microfluidic magnetic cell sorting, the prototype cell sorter was made from photoresist. The material permitted quick fabrication of channels that could also be rapidly duplicated for experimentation using projection photolithography

(light etching). The layers of the device are shown in Figure 11a. Patterns of arrays of magnetic disks were etched using electron beam lithography (Focused Ion Beam/ Scanning Electron Microscope) at the Ohio State University Center for Electronic & Magnetic Nanoscale Composite Multifunctional Materials (ENCOMM) NanoSystems Laboratory (ENSL). Permalloy was sputtered onto the disk array pattern using the AJA Sputter Tool at Nanotech West. Greg Vieira and Tom Henighan fabricated the disk arrays.

The following procedures were carried out in the Photo Lab of the ENSL:

Silicafilm (SiO_2; Emulsitone Company) was deposited on top of the disk array to protect the disks from damage due to the moving fluid of the microfluidic device. For a 200 nm layer, the silicafilm was spin-coated at 3000 rpm for one minute and then baked at 180^{o}C for 15 min. After the substrate was allowed to cool, SPR-220-7.0 (Megaposit; Rohm and Haas) was spin-coated at 1200 rpm for one minute and then baked at 110^{o}C for 2.5 min, producing a 15- 20 μm thick layer.

Photomasks for the microchannel construction were fabricated on lithographic films. The film was exposed under bright white light for 10 s. Immediately after, the film was developed (Kodak Super RT Developer) for 3 min, then washed in a stopper (Kodak Indicator Stop Bath) for 30 s, washed in a fixer (Kodak Professional Rapid Fixer) for 5 min, and finally rinsed with distilled water.

A T-shape photomask was aligned with the disk array so that the disks would facilitate transportation into the branch channel, as shown in Figure 11b. The T-junction pattern in the SPR-220 photoresist was exposed under white light for 1 min through the 100x objective of an Olympus BH2-UMA microscope and developed by soaking for 30 s

in MF-24A developer (Megaposit; Rohm and Haas) while agitating the sample. During exposure, maximum light intensity of the Olympus TH3 power supply was used, and the disks at the bottom of the photoresist along with the projected photomask pattern were in focus of the microscope.

Exposing straight-line photomask patterns beginning from the 3 ends of the T-shape junction extended the T-junction microchannel. Each extension exposure was done for 40 min and after all 3 extensions were exposed, the wafer was developed for 4 min. The extensions allowed for the introduction of solution by pipette and allowed the fluid reservoirs to be far enough away from the Leica microscope objective field of view when observing the T-junction during an experiment.

Holes were introduced in a polydimethylsiloxane (PDMS) polymer slab to serve as fluid reservoirs, as depicted in Figure 11c. The PDMS cover was pressed onto the photoresist, creating a temporary seal. For the experiment, solutions were introduced into the reservoir ports. Fluid flow was controlled by a gravitational pressure gradient among the 3 reservoirs of the microchannel, based on the amount of fluid in each reservoir. The magnetic manipulation technique was used to separate magnetic beads from nonmagnetic particles, which followed the fluid flow into the output channel while magnetic bead were transported into the branch channel.

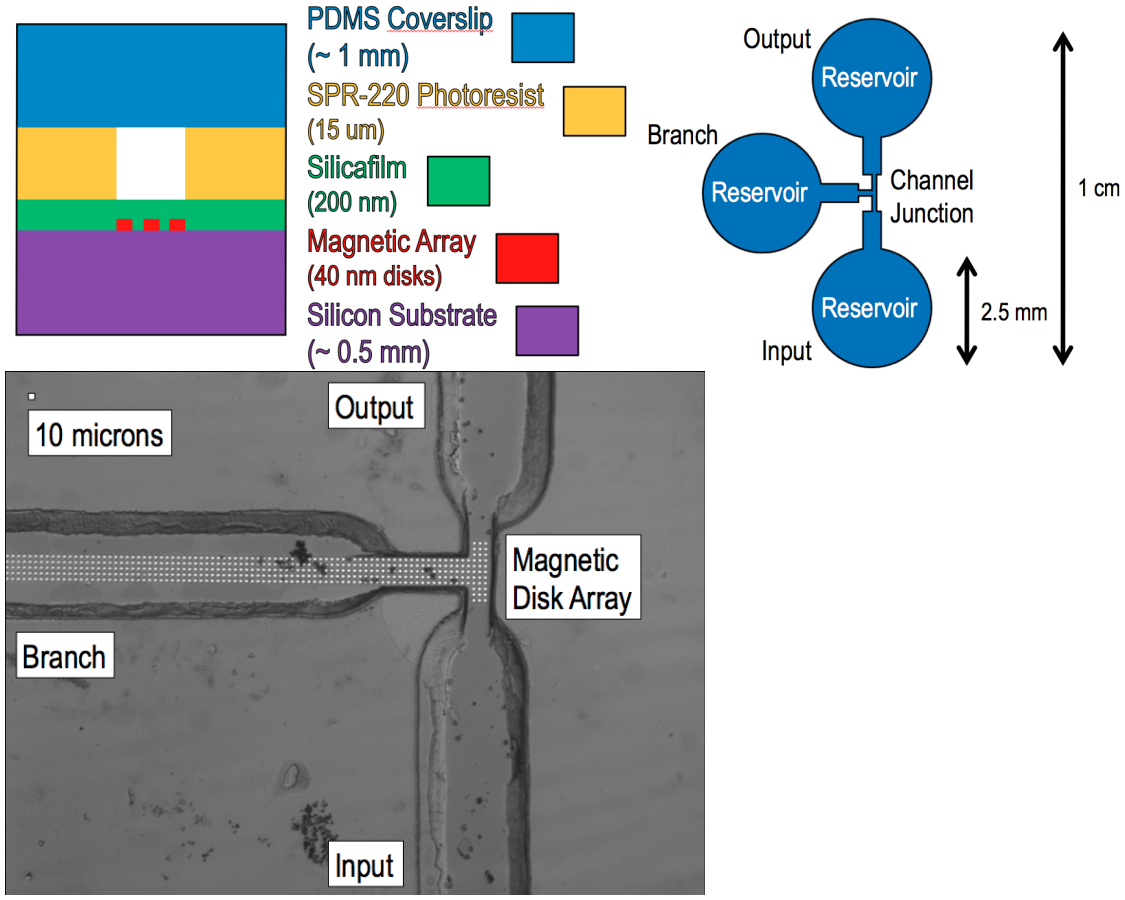

Figure 13. (Top Left) Diagram of layers of prototype photoresist device.
(Top Right) Device layout, top-view.
(Bottom) Picture of T-channel junction. White dots are magnetic disks at the junction. Solution flows up from the input. Magnetically labeled cells are transported to the left (branch channel), while nonmagnetic particles follow the fluid flow up toward the output.

B. Preliminary PDMS Device

HyunChul Jung in Dr. Wu Lu's group fabricated this device.

After preliminary success with cell separation using the prototype photoresist cell sorter, a new device was fabricated out of PDMS. This allowed for the application of surface treatments to reduce cell-to-channel surface adhesion—treatments which require solvents that would have worn away and destroyed the photoresist material. Additionally, the permanent PDMS to Si bond allowed for the use of syringe pumps to control fluid

flow, the pressure of which would have caused the temporary seal of the prototype device to leak.

As shown in Figure 12, after the disk array (5 µm diameter, 5 µm spacing in between disks) was imprinted on the Si wafer and a layer of SiO_2 deposited to protect the disks from the fluid flow (carried out by Greg Vieira), a layer of Au was sputtered in the pattern of the microchannel bottom. The Au coating allowed for a polyethylene glycol-thiol (PEG-SH) surface treatment to reduce cell adhesion by making the surface hydrophilic. A PDMS channel mold was then aligned to the Au coating and permanently bonded to the SiO_2 layer. Tubing connected the microchannel ports to syringe pumps for fluid flow control.

Knowledge gained experimenting with parameters of this device and the success of cell separation using this device permitted the next step of integrating two parts of a "lab-on-a-chip" microfluidic device: cell separation and encapsulation in oil droplets.

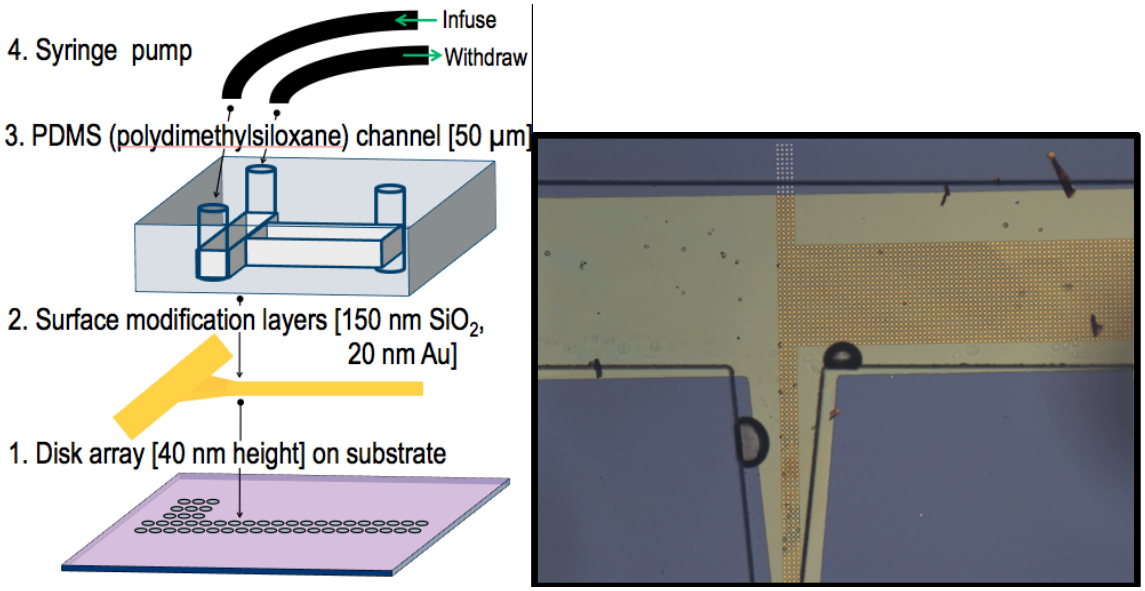

Figure 12. Diagram of microfluidic device side-view (Left) and picture of device top-view (Right).

C. Figure Sources

Figure 1, page 4. Thanks to Tom Henighan and Aaron Chen for the diagram and picture.

Figure 2, page 5. Thanks to Tom Henighan and Aaron Chen for the energy landscape and instructions to run OOMMF simulation.

Figure 3, page 6. Thanks to Tom Henighan for the original animation.

Figure 4, page 7. Thanks to Aaron Chen and Brandon Miller for the diagrams.

Figure 5, page 8. Thanks to Aaron Chen for the picture.

Figure 6, page 12. Thanks to Aaron Chen for the picture.

Figure 12, page 30. Thanks to Greg Vieira for the picture.